# Feasibility of a synchrotron storage ring for neutral polar molecules

Hiroshi Nishimura*
*Mail Stop 80-101, Lawrence Berkeley National Laboratory, University of California, Berkeley CA 94720*

Glen Lambertson,† Juris G. Kalnins,‡ and Harvey Gould§
*Mail Stop 71-259, Lawrence Berkeley National Laboratory, University of California, Berkeley CA 94720*
(Dated: May 10, 2003)

Using calculations and mathematical modeling, we demonstrate the feasibility of constructing a synchrotron storage ring for neutral polar molecules. The lattice is a racetrack type 3.6 m in circumference consisting of two of 180-degree arcs, six bunchers, and two long straight sections. Each straight section contains two triplet focusing lenses and space for beam injection and experiments. The design also includes a matched injector and a linear decelerator. Up to 60 bunches can be loaded and simultaneously stored in the ring. The molecules are injected at 90 m/s but the velocity of the circulating beam can be decelerated to 60 m/s after injection.

The modeling uses deuterated ammonia ($^{14}N^2H_3$) molecules in a weak-field seeking state. Beam that survives 400 turns (15 s), has horizontal and vertical acceptances of 35 mm-mr and 70 mm-mr respectively, and an energy acceptance of $\pm 2\%$.

PACS numbers: 29.20 Dh, 41.75.Lx, 33.80.Ps, 39.90.+d, 33.55.Be

## I. INTRODUCTION

Charged particle storage rings are used: to accumulate particles, to adjust their energy, to store and maintain them for cooling, and to increase the particle flux compared to single pass devices. In this paper we examine the feasibility of constructing a synchrotron storage ring for neutral polar molecules that could be put to these uses. The specific application is for slow, cold molecules which are now beginning to be studied and which are not easily produced in large numbers [1–4]. As molecules that have been slowed are easier to deflect and focus, a very compact storage ring may be designed.

Neutral polar molecules are deflected and focused by forces from electric guide fields acting upon their electric dipole moments. A uniform field produces an effective electric dipole moment in the molecule but, unlike a charged particle, produces no body force. The effective dipole moment depends upon the magnitude of the electric field and upon the molecular state. (This would be equivalent, in charged particle optics, to a particles charge depending upon the electric potential.) The force, $F_x$, in the (transverse) $x$ direction is:

$$F_x = -\frac{\partial W}{\partial x} = -\frac{dW}{dE}\frac{\partial E}{\partial x} \tag{1}$$

where $W$ is the potential energy, in an electric field of magnitude $E = (E_x^2 + E_y^2)^{1/2}$. A similar expression may be written for the force in the $y$ direction. $-\partial W/\partial E$ is the effective dipole moment. In a nonuniform electric field, the rotational state of the molecule (and sometimes the magnitude of the electric field) determines the sense of the force - either toward or away from the stronger total field. In this study we chose a molecular state for which the force is toward the weaker field.

Only the magnitude, not the direction, of the electric field acts to produce force. Thus, one uses combinations of dipole, quadrupole, and sextupole fields but in contrast to charged particles the forces are quite different. With the addition of a quadruple field component, to a dipole field, the resulting gradient exerts a deflecting force plus focusing forces in the direction normal to the deflection; this can be used as a bending element. A sextupole added to a uniform electric field produces gradients in the total field that give focusing in one direction and defocusing perpendicular to that. Thus, this sextupole-dipole combination is used much like the quadrupole in the case of charged particles. But unlike charged particles, these gradient-induced focusing forces on the molecule are not linear for large excursions. Some adjustment of nonlinearities are achieved by adding higher-multipole components but the inherent nonlinearities are a challenge in the design of the guide fields for neutral molecules.

Forces in the direction of the molecules forward motion are produced by having the molecule enter or exit regions of higher electric field [2, 5, 6]. Again, the field can be perpendicular to the motion of the molecule as only the magnitude, not the direction, of the field acts to produce force. While in the gap between parallel electrodes, the field may be increased with no effect on the molecule because a uniform time-varying electric field does no work on the molecule. However, upon exiting that higher field, the molecule will be accelerated; this action of pulsed electrodes can be applied repeatedly and used as a decelerator (accelerator) or as a buncher.

Prior to this study, a continuous torroidal ring, without a buncher or matched injector was suggested by Auerbach et al.[7], analyzed by Katz[8], and Loesch and Schell [9], and recently constructed by Crompvoets et al.[10], who captured single pulses (about $10^6$ molecules) of $^{14}N^2H_3$ at 90 m/s (kinetic energy $\approx 9.7$ K) and observed them for six turns (0.053 s).

A ring with much longer storage times that can capture and store the high peak intensity of (the decelerated output of) a pulsed molecular beam jet source provide a larger flux. With

*E-mail:H_Nishimura@lbl.gov
†E-mail:GRLambertson@lbl.gov
‡E-mail:JGKalnins@lbl.gov
§E-mail:HAGould@lbl.gov

bunching, the energy of the stored beam can be varied continuously and the density of the molecules varied. These features make a molecular synchrotron storage ring useful for high-resolution spectroscopy, low energy scattering experiments, and for evaporative cooling [11, 12]. With evaporative cooling, the molecules can reach ultra-low temperatures where they may form quantum condensates.

Evaporative cooling requires: high densities to thermalize the molecules by elastic scattering, forced evaporation of the hottest molecules, and long storage times for many repetitions of the cooling cycle. In this process bunching (and focusing) raises the density to thermalize the molecules and beam drift (and/or debunching) isolates the hottest molecules for removal.

The results of our study show that it is feasible to construct a molecular synchrotron storage ring that will capture large numbers of molecules in multiple bunches, maintain the bunches, store the molecules for longer than 15 seconds and vary their kinetic energy. The acceptance of the storage ring and decelerator scale with their size, with allowance for nonlinearities and the voltage limits of large electrode gaps. The storage ring and decelerator modeled here are matched and are of a size that is typical for laboratory apparatus. The particular example described in this paper may stimulate interest in specific features of such a facility from which exact specifications would emerge and be pursued in it's own design study.

The paper is organized as follows: In section II we discuss the lattice, the choice of molecular state, the necessity of avoiding regions of very weak electric field, and the dynamics calculations. In section III we describe the performance of the synchrotron storage ring, including the dynamic aperture, operating parameters, the effect of gravity, bunching and deceleration, and collisional losses. Finally, in section IV we evaluate the overall performance of the storage ring by adding a molecular beam source, a linear decelerator, and an injection system.

## II. STORAGE RING DESIGN

### A. Lattice

Many different designs and placements of the elements were considered and analyzed. Our resulting design (Fig.1) is a racetrack configuration consisting of two of 180-degree arcs, 4 triplets of focusing lenses, six bunchers placed in regions having low horizontal dispersion, an injector for loading up to 60 bunches into the ring, space in the long straight sections for an extractor (for example a mirror image of the injector), and for experiments or evaporative cooling. The lengths of the elements and drift distances between them are listed in Table I. The strong combined horizontal and vertical focusing in the bend sections makes the ring very compact. The triplet of straight-lens electrodes then transforms the beam to a wider, more collimated beam that can traverse the 32-cm-long straight section as shown in Fig. 2(a). The large variation of focusing strength is apparent in Fig. 2(b), the plot of the focusing parameters $\beta_x$ and $\beta_y$ around the ring.

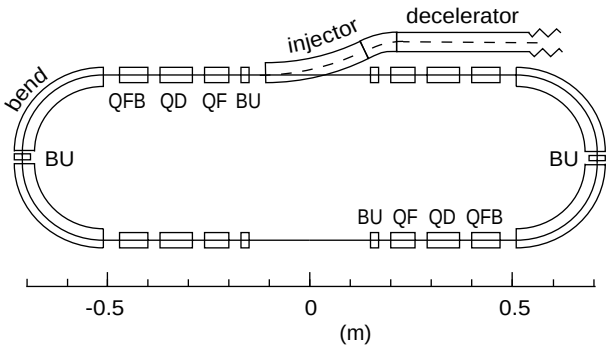


FIG. 1: Schematic diagram of the synchrotron storage ring modeled in our study. The bend radius is 0.2 m and the circumference is 3.36 m. QF and QBF are horizontal focusing (vertical defocusing) lenses, QD are horizontal defocusing (vertical focusing) lenses and BU are bunchers. The injector and a portion of the decelerator are also shown. Additional details of the lattice are found in Table I, details of the focusing lenses and bend elements are found in Table II and Fig.'s 5, 6. Details of the decelerator and injector are found in sections IV A and IV B respectively.

TABLE I: Element length and placement for one-fourth of the lattice

| Element | Length (cm) | Cumulative travel (cm) |
|---|---|---|
| Drift | 16.0 | 16.0 |
| Buncher (BU) | 2.0 | 18.0 |
| Drift | 2.0 | 20.0 |
| QF | 6.0 | 26.0 |
| Drift | 3.0 | 29.0 |
| QD | 8.0 | 37.0 |
| Drift | 3.0 | 40.0 |
| QFB | 7.0 | 47.0 |
| Drift | 4.0 | 51.0 |
| $90^o$ Bend | 31.4 | 82.4 |
| Drift | 0.5 | 82.9 |
| Half buncher (BU) | 1.0 | 83.9 |

The horizontal betatron phase advance in the 180-degree bending region has been made equal to $4\pi$ in order to have zero dispersion at the bunching electrode, as shown in Fig. 3. The very low dispersion at the bunching electrodes prevents the development of strong synchro-betatron coupling and preserves the momentum acceptance.

### B. Molecular state

Many different molecules and kinetic energies could be used for our feasibility study. We selected 90 m/s $^{14}N^2H_3$ molecules in the weak-field seeking upper-inversion level (lowest vibrational state) $|J,K,M>=|1,1,-1>$ (Fig. 4) because they had been previously used by Crompvoets et al.[10], and because the focusing properties of weak-field seeking states make the design and feasability assessment easier and the ring more compact.

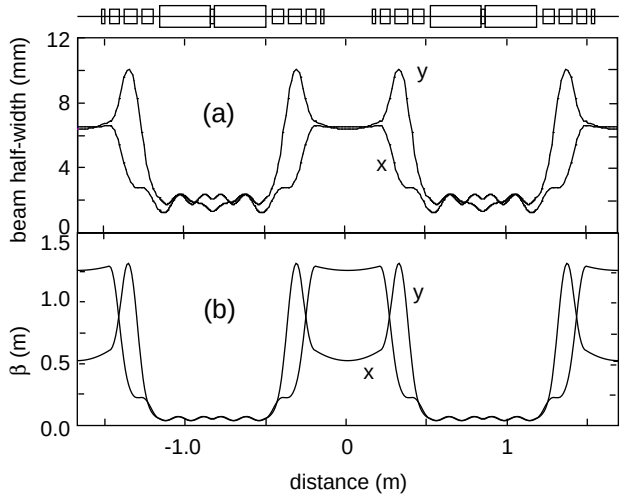


FIG. 2: Beam envelope (a) and focusing parameter β (b) in the horizontal ($x$) and vertical ($y$) directions. β is the distance in which the transverse (betatron) oscillation advances in phase by one radian. A schematic of the lattice is shown above for location reference.

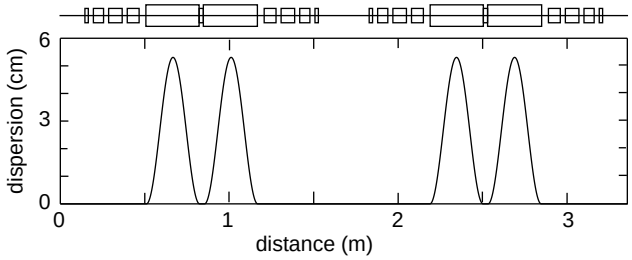


FIG. 3: Horizontal dispersion of the beam around the lattice. Low dispersion at the bunchers prevents the development of synchro-betatron oscillations.

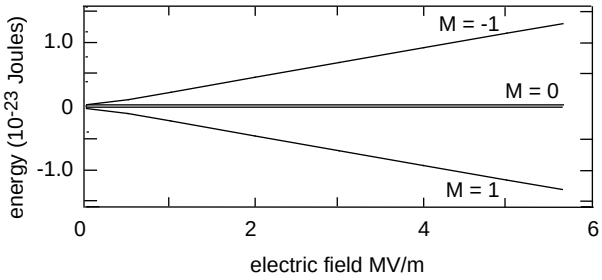


FIG. 4: Stark effect in the $|J,K>=|1,1>$ levels of $^{14}N^2H_3$. The $M=-1$ level is weak-field seeking and used for this study. Inversion splitting, dipole moment and rotational constant are taken from Townes and Schawlow [13].Hyperfine splitting and the Stark effect in the $10^{-24}$ Joule inversion-split $M=0$ levels are neglected.

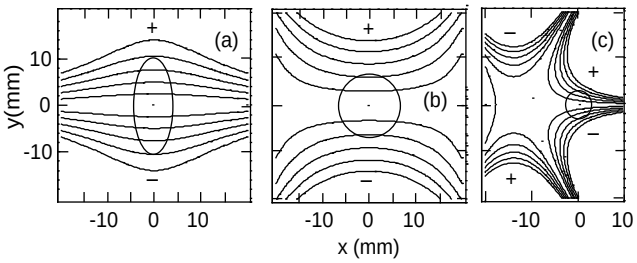


FIG. 5: Maps of (truncated) equipotentials in $x$ and $y$ of (a) F lenses, QF and QFB (horizontal focusing, vertical defocusing), (b) D lenses, QD (horizontal defocusing, vertical focusing), and (c) bend elements (horizontal and vertical focusing). The ellipse and circles show the approximate size of the beam envelope in the element. Note that the electric field direction at the orbit of the molecules is always in the vertical direction. The actual electrode can be fabricated to lie along any set of equipotentials that are larger than the beam size.

Molecules in weak-field seeking states (molecules whose potential energy increases in an electric field) can be focused simultaneously in both transverse directions, whereas molecules in strong-field seeking states can be focused in only one transverse direction while defocusing in the other transverse direction.

Fringe fields seen by the molecules upon entering and exiting the bending, focusing, and bunching elements will also exert transverse forces on the molecules. A molecule in a weak-field seeking state traveling in the $z$ direction will experience a net focusing effect in the vertical ($y$) direction upon entering or exiting an electric field produced by horizontal ($x,z$) plane parallel electrodes. A molecule in a strong-field seeking state will defocus.

Except for the rotational state $J=0$ (which is always strong field seeking), each rotational state, $J$, contains $M$ components which are partially or completely degenerate in zero electric field. The different $|M|$ states (or $M$ states as in Fig. 4) have different Stark shifts and hence experience different forces in an electric field gradient. If the molecules in a ring repeatedly enter regions of weak and direction-changing electric fields, transitions between the different $M$ components will take place (Majorana transitions), leading to a loss of the molecules[14–16]. Our method of avoiding this problem is described below.

### C. Avoiding weak-field regions

In the bend sections, which use electrodes with zero electric field near their center, the centripetal force keeps the trajectory of molecules in a strong electric field at the inner side of that zero (Fig. 5c). And, as did Crompvoets et al.[10], we take advantage of the combined horizontal and vertical focusing.

Focusing lenses in the straight sections (Fig. 5a,b) are sextupolar with a dipole field added to avoid zero field. The multipole coefficients of the electrodes, their gaps, and electric field strengths on orbit, are listed in Table II. With the added dipole field, these lenses focus in only one transverse direction while defocusing in the other and are used in an alternating-gradient sequence [17]. To prevent rapid changes in electric field direction, the field direction, at the molecule's orbit throughout the ring, is vertical and remains unchanging in polarity (Fig. 6). This results in having some concave and some convex lenses.

TABLE II: Bending and focusing/defocusing electrodes

| Electrode | Length (cm) | $E_0$ (MV/m) | Half-gap (mm) | $A_2$ | $A_3$ |
|---|---|---|---|---|---|
| bend | 31.4 | 3.37 | 6 | 157 | 5667 |
| QF | 6.0 | 2.88 | 15 | 0 | 2000 |
| QD | 8.0 | 3.55 | 15 | 0 | -2000 |
| QFB | 7.0 | 4.30 | 15 | 0 | 2000 |

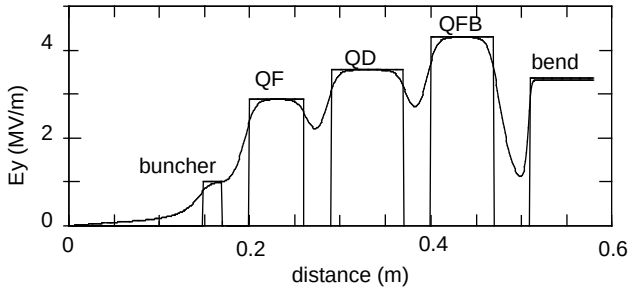


FIG. 6: Electric field magnitude around the ring. All electric fields are in the vertical direction and do not change sign. The buncher field is shown for an on-energy molecule entering or exiting the buncher (see section III C). The fringe fields are part of the focusing system and are discussed in section II D 3.

In the straight sections, away from focusing fields, we add a weak bias field (about one kV/m for the drift spaces) to maintain the quantization axis[15].

### D. Dynamics calculation

The force on a molecule in one direction is given by Eq. 1. The basic formulas for motions of the molecules are derived analytically without linearization. Then the beam optics and dynamics are numerically calculated and optimized by using a modified version of the program Goemon[18] that was originally developed for relativistic charged particles. The molecules were numerically tracked through the synchrotron for 400 turns (15 s) to determine the beam's dynamic stability.

The numerical integration was done in the time domain because the speed of a molecule varies as a function of the electric field. The overall dimension of the lattice is chosen to balance easily attainable electric fields and high transverse acceptance with compact (desk top) size.

#### 1. Potential energy

The potential energy, W, in an electric field, of the $|J,K>=|1,1>$ level of $^{14}N^2H_3$ (Fig. 4) is given, in units of Joules (written out to avoid confusion with the quantum number "$J$") by:

$$W = \pm\left[\sqrt{C_1^2 + C_2^2E^2} - C_1 - C_3E^2\right]$$

where $C_1 = 5.26\times10^{-25}$Joules is half of the $|J,K>=|1,1>$ inversion splitting (Fig. 4), $C_2 = 2.52\times10^{-30}$JoulesV$^{-1}$m, $C_3 = 1.78\times10^{-38}$JoulesV$^{-2}$m$^2$ and $E$ is in V/m. The terms involving $C_1$ and $C_2$ are taken from Ref.[13] to which we add a second order term to account for mixing of the $|J,K>=|2,1>$ state in strong electric fields[19].

#### 2. Electric field gradient

Within an electrode, the electric field, as a function of distances $x$ and $y$ from the reference orbit, is calculated from a scaler potential $\psi$ by $E = -\nabla\psi(x,y)$ and $\psi$ is taken to be uniform in the longitudinal ($z$) direction within the electrode length. The fringe fields, at the ends of the electrodes, where the electric field is changing in the $z$ direction of motion produce additional transverse forces. These are evaluated separately, and are described in section II D 3.

In a straight (focusing/defocusing) electrode, the potential is a combination of dipole and sextupole terms [17] given by $\psi_s = -E_0[y + A_3(x^2y - \frac{1}{3}y^3)]$ where $E_0$ is the central electric field, $A_3$ is the sextupole coefficient (see Table II) and the dipole coefficient has been set equal to 1.

In a bending electrode of constant radius $\rho$, $\psi$ is a combination of dipole, quadrupole, and sextupole terms given by:

$$\psi_b = -E_b\left[y + yB_2\ln\left(1+\frac{x}{\rho}\right) + B_3J_0[k(\rho+x)]\sinh(ky)\right]$$

Relating this to the Cartesian multipoles, we find: $E_b = E_0\left[1+2A_3/k^2\right]$, $B_2 = \rho A_2\left[k^2/k^2+2A_3\right]$, where $A_2$ is the quadrupole coefficient,

$$B_3 = -\frac{1}{kJ_0(k\rho)}\frac{2A_3}{k^2+2A_3},$$

$J_0$ and $J_1$ are the $0^{th}$ and $1^{st}$ order Bessel functions and the value of $\rho k$ is the first root of $J_1(k\rho) = 0$. An approximation for $\psi_b$ useful for comparison with $\psi_s$ up to third order is

$$\psi_b = -E_0\left[y + A_2xy + A_3\left[\left(1-\frac{A_2}{2\rho A_3}\right)x^2y - \frac{y^3}{3}\right]\right]$$

#### 3. Fringing fields

To evaluate the transverse vertical focusing forces in the fringing regions of the elements, a two - dimensional numerical calculation, using the geometries of the electrodes, was carried out to find the electric field as a function of z on the midplane. The magnitude of the fringe fields are shown in Fig. 6. The focusing action was then calculated analytically from the derivatives of this field, evaluated as equivalent thin lenses at the ends of the focusing, bending, and bunching electrodes, and included in the calculation of trajectories around the ring.

#### 4. Hamiltonian

All optics, orbit, and tracking calculations were carried out using a second-order symplectic integrator and the Hamiltonian: $H = H_0 + W(x,y)$. In straight regions, $H_0 = \frac{1}{2m}(P_x^2 +$

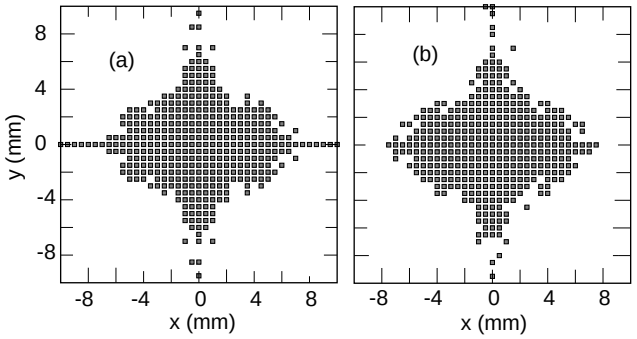


FIG. 7: Dynamic aperture for on-momentum molecules: the starting coordinates for the molecules that survive 400 turns (a) without gravity and (b) with gravity. Dynamic aperture is the area, in the transverse plane, at the center of the long straight section, occupied by the molecules.

$P_y^2 + P_z^2$) where $m$ is the mass of the molecule, $P_x = mv_x$, $P_y = mv_y$, and $P_z = mv_z$ is the momentum, with $v_x$, $v_y$, and $v_z$ the velocities in Cartesian coordinates. Conservation of energy requires that $P_z$ changes when the molecule passes through a field gradient at the ends of the electrodes.

In a bending region, the Hamiltonian $H_0$ becomes:

$$H_0 = \frac{1}{2m}\left[P_x^2 + P_y^2 + \frac{P_\theta^2}{(\rho + x)^2}\right]$$

where $P_\theta$ is an angular momentum, $\rho$ is a reference bend radius, $x$ is a radial excursion with respect to $\rho$, and $P_z = (P_\theta/\rho + x)^2$.

## III. SYNCHROTRON PERFORMANCE

### A. Dynamic aperture

The survival of molecules, tracked through 400 turns, is calculated to determine the usable dynamic apertures, $a_x$ and $a_y$. Fig. 7 shows a scatter plot of the starting coordinates $x$ and $y$ at center of the straight section of those molecules that survive the 400 turns. From these we calculate the acceptances, $\varepsilon$, as $1/\pi$ times the areas in displacement-angle phase space, $\varepsilon = a^2/\beta$. The dynamic apertures, values of beta at center of straight section, and acceptances are given in Table III. In Table III the circulation period is 38 ms whereas 3.357/90=37.3 ms, reflecting the 3% to 4% reduction in velocity when the molecules enter the electric fields.

The dynamic aperture of off-momentum molecules determines the momentum acceptance. Fig. 8 shows the effect of momentum on the dynamic aperture, and indicates an acceptance of about -3% to +1.7%. We shall see later that this reduces to about $\pm$2% when the bunchers are operating.

The betatron tunes, as a function of momentum, are found by tracking the motions of a molecule over 512 turns. The chromaticities, are $\zeta_x = -0.0885$ and $\zeta_y = -0.0942$. The effect of momentum-deviation upon the circulation period T, expressed as the momentum-compaction factor $\alpha$ in $\Delta T/T_0 = \alpha\Delta P/P_0$, is strong. The value of $\alpha$ is -0.991; this will result in prompt debunching if the bunching voltages are turned off.

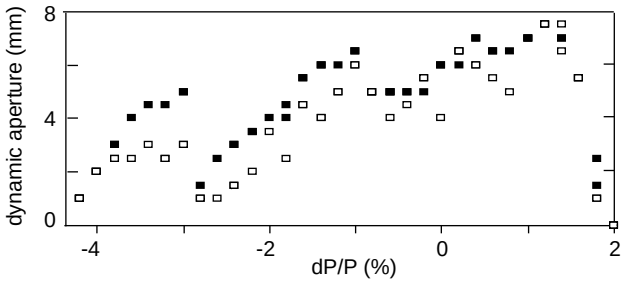


FIG. 8: Dynamic aperture as a function of momentum variation from the nominal tune for $x$ (solid points) and $y$ (open points) with gravity but without bunching. The molecules in Fig. 7 appear here at dP/P = 0.

TABLE III: Synchrotron operating parameters

| | |
|---|---|
| Circumference (m) | 3.357 |
| Circulation period (s) | 0.0380 |
| Velocity in free space (m/s) | 90.0 |
| Beta horizontal [a]: $\beta_x$ (m) | 1.264 |
| Beta vertical [a]: $\beta_y$ (m) | 0.513 |
| Horizontal dispersion[a] (m) | 0.001 |
| Horizontal tune: $\nu_x$ | 5.250 |
| Vertical tune: $\nu_y$ | 5.200 |
| Chromaticity - horizontal: $\zeta_x$ | -0.0885 |
| Chromaticity - vertical: $\zeta_y$ | -0.0942 |
| Momentum compaction: $\alpha$ | -0.99 |
| Dynamic aperture - horizontal: $a_x$ (mm) | 6.5 |
| Dynamic aperture - vertical: $a_y$ (mm) | 6.0 |
| Acceptance - horizontal: $\varepsilon_x$ (mm - mr) | 35 |
| Acceptance - vertical: $\varepsilon_y$ (mm - mr) | 71 |

[a] At the center of the long straight section.

### B. Effect of gravity

The effect of gravity is visible in the orbit because the velocity of the beam is low. The vertical phase advance of $4\pi$ (same as the horizontal phase advance), is favorable in reducing the effect of the gravity force on the vertical closed orbit. Fig. 9 shows the vertical closed-orbit displacement (COD) due to gravity. It ranges from -0.13 mm to 0.09 mm and is small enough to be neglected in the case of linear optics calculations. In the case of dynamic aperture calculations we have confirmed that gravity changes only the details of the dynamic aperture at its edges and does not affect its core portion (Fig. 7).

### C. Bunching and deceleration

Bunching action is provided by six sets of parallel-plate electrodes, each 20 mm in length with 10 mm half-gap, placed

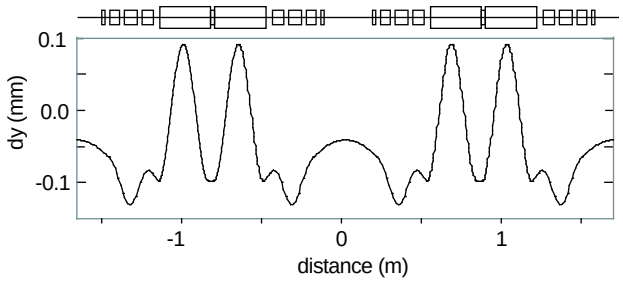


FIG. 9: Closed orbit displacement (COD) from the reference orbit due to gravity. The swings of the COD in the bending sections are similar to the curve of the horizontal dispersion because the vertical and horizontal betatron tune advances are both $4\pi$.

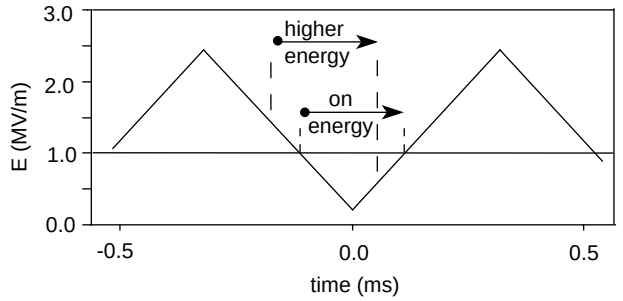


FIG. 10: Buncher timing for an on-energy molecule and a faster molecule. Changing the buncher timing may be used to change the circulating beam energy.

in low dispersion regions around the ring (Fig.1, 3). The voltage on the plates is pulsed in a triangular waveform that produces a maximum electric field of 1.0 MV/m for on-energy molecules. Each buncher is synchronized to the on-energy molecules (Fig. 10) so that the energy lost upon entering the buncher is matched by the energy gained upon exit. A higher-energy molecule reaches the buncher at an earlier time when electric field gradient is higher upon entrance and lower upon exit, resulting in a net energy reduction for a molecule in a weak-field seeking state. The survival of the molecules, in the storage ring, including the effects of bunching and gravity is shown in Fig. 11.

The buncher frequency is 1.58 kHz and allows 60 bunches around the ring, spaced 56 mm apart. To prevent Majorana transitions the voltage is biased to avoid negative fields. The rate of change of the electric field in the bunchers can be made as large as about 7 $\mathrm{GVm^{-1}s^{-1}}$. The synchrotron tune is proportional to the square root of the rate of change and is 0.92 at our reference value of 7 $\mathrm{GVm^{-1}s^{-1}}$.

The lattice is optimized for a nominal velocity of 90 m/sec. After stacking at this velocity, the beam can be decelerated by synchronously changing the electrode and buncher settings. This provides an opportunity to scan the velocity during an experiment. The betatron tunes stay constant but the straight section becomes dispersive. At 63 m/sec, the horizontal transverse acceptance reduces from 35 to 13 mm-mrad and the momentum acceptance from 2.0% to 1.2%.

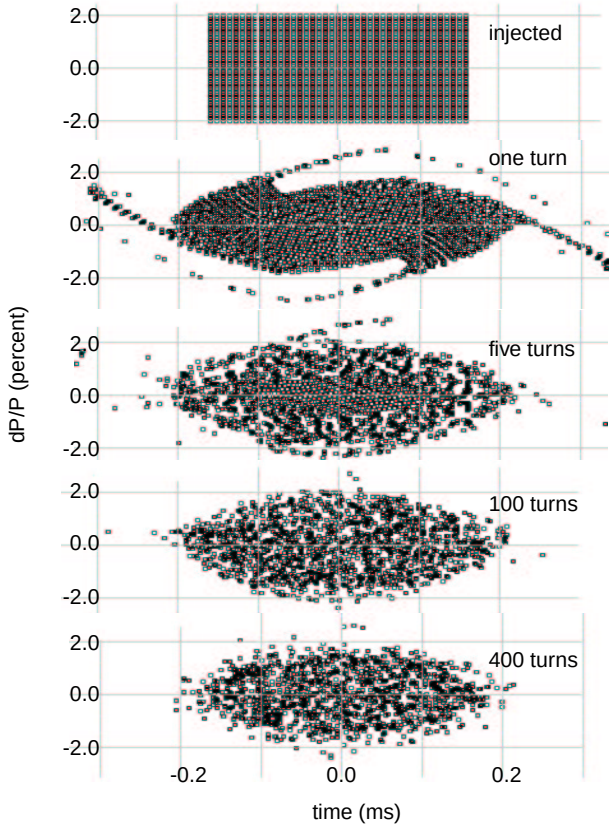


FIG. 11: Scatter plot of an initially injected $\pm 158\mu$s-long pulse of molecules with a $\pm 2\%$ momentum spread after 1 - 400 turns. The velocity spread of $\pm 1.8$ m/s represents an energy spread in the moving frame of about $\pm 0.4$ K.

### D. Collisional losses

So far, we have only examined storage ring losses associated with the limits of the dynamic aperture and momentum acceptance of the lattice. A real storage ring will also have losses due to elastic and inelastic scattering of the molecules. Scattering by room-temperature background gasses is the major elastic scattering contribution and of the gasses likely to be present in the ring, xenon and ammonia have the largest scattering coefficients. Assuming hard sphere binary collisions between the $^{14}N^2H_3$ molecules and 300 K xenon (leaking in from the source), the mean time between collisions is 15s at a (xenon) pressure of $1 \times 10^{-7}$ Pa ($7.5 \times 10^{-10}$ Torr), where we have used the equations and collision diameter in Ref.[20].

For inelastic scattering between the $^{14}N^2H_3$ molecules, their relative kinetic energy spread of about $\pm$ 0.4 K ($\pm 5.5 \times 10^{-24}$J) is small enough to prevent any significant excitation to higher rotational states. A molecule can however collisionally relax to a strong-field seeking state, causing it to be lost from the storage ring [10]. Bohn [21] and Kajita [22] have calculated inelastic collision rates for molecules in a weak-field seeking state in electrostatic traps. They find that the loss rates can be significant, in some cases precluding successful evaporative cooling, and are influenced both by the electric fields

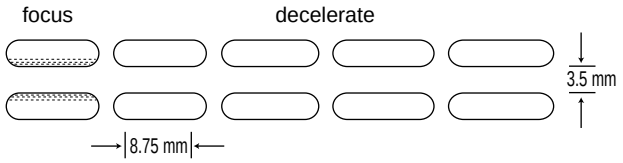


FIG. 12: Last elements of a linear decelerator showing a group of four decelerating electrodes and one focusing lens. The lengths of the decelerating elements and focusing lenses decrease to match the velocity of the decelerating molecules.

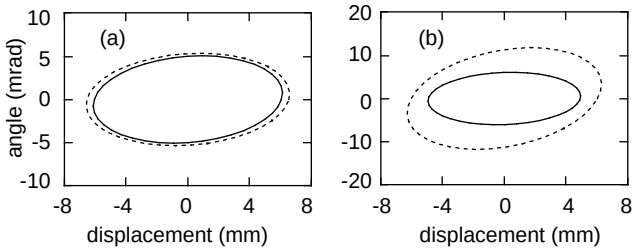


FIG. 13: Boundaries of injected-beam emittances (solid lines) and storage ring acceptances (broken lines) in the (a) horizontal and (b) vertical planes.

and the size of the electric dipole moment.

Thus, the use of a synchrotron storage ring with high densities of molecules in a weak-field seeking state will need to confront this issue. Obviously, the alternative would be to use molecules in the strong-field seeking rotational ground ($J = 0$) state. A synchrotron storage ring for molecules in the $J = 0$ state will be discussed in a future paper.

## IV. SYNCHROTRON STORAGE RING SYSTEM

The overall performance of a molecular synchrotron storage ring also depends upon the beam delivered by the source, decelerator and injection line. To model performance and determine the stored beam from the complete system we also modeled a decelerator, injector and source.

### A. Linear decelerator

Slow molecules, suitable for injection into a storage ring, can be produced by time-varying electric field gradient deceleration, by mechanical cancellation of the molecular beam velocity[3], and possibly by buffer-gas cooling[1] (without magnetic trapping). Time-varying electric field gradient deceleration is the easiest of these for us to model and to match to the storage ring. It has been used by Bethlem et al. [23, 24] and Crompvoets et al. [10] to decelerate $^{14}N^2H_3$.

Our model linear decelerator takes the 310 m/s (115 K kinetic energy) output of a $^{14}N^2H_3$ - seeded xenon pulsed-jet source (room temperature reservoir) and decelerates it to 90 m/s (9.75 K kinetic energy). The number of electrodes is set by the decrease in kinetic energy in each electrode (equal to the change in potential energy of the molecule entering the electric field). We use 79 decelerating electrodes, decreasing in length from 48 mm to 8.75 mm effective length to keep the transit time of the molecules constant through each electrode. We choose the overall length of the decelerator, 3.4 m, comparable to the 3.36 m circumference of the storage ring, to balance high velocity acceptance with compact size.

The electric field is nearly a square wave 158 $\mu$s long with a repetition rate of 3.16 kHz and the maximum electric field is 8 MV/m in a 1.75 mm half-gap and is the same for all decelerating electrodes. After the molecules enter the electric field it drops to nearly zero so that the molecules that exit the electrode must relinquish kinetic energy to enter the field in the next set of electrodes. This is done either by having successive electrodes 180 degrees out of phase or by using only every other bunch. The electric field does not return completely to zero and the horizontal focusing elements (see below) have their electric field in the same direction as the decelerating electrodes to minimize Majorana transitions.

Bunching, as the molecules decelerate, is accomplished by having the electric field (in each bunching electrode) decrease, linearly over the 158 $\mu$s from 8 MV/m to 7.76 MV/m so that the fastest molecules, arriving early, receive the most deceleration. This results in a $\pm 1\%$ momentum spread at 90 m/s which falls within the momentum acceptance of the storage ring.

The spacing between individual decelerating electrodes remains constant. This fixes the fringe field which provides vertical focusing. The decelerating electrodes are grouped in sets of four as shown in Fig. 12. After each quadruplet of decelerating electrodes is placed a horizontal focusing element with length appropriate to keep the molecules in phase with the next decelerating quadruplet. (One section has only three decelerating electrodes.) The 20 focusing elements all have the same field but their focusing strength increases as the molecules slow. The lattice is, in the vertical direction, FFFFD and in the horizontal direction OOOOF. The overall length of the decelerator is 3.4 m.

Upon exit from the decelerator, bunches are 7 mm long with a vertical and horizontal half-width of 1.30 mm and 1.61 mm, respectively. The vertical and horizontal betas are: $\beta_v = 56.3$ mm and $\beta_h = 86.7$ mm corresponding to vertical and horizontal emittances both of 30 mm-mr. Being less than the 71 mm-mr and 35 mm-mr vertical and horizontal acceptances of the synchrotron storage ring, this sets the overall transverse acceptance of the entire system.

### B. Injector

A bunched beam of molecules is injected onto the closed orbit of the synchrotron at the downstream end of a straight section. Starting at the exit of the decelerator, this beam is guided along a trajectory by electric fields that focus transversely and transform its size and divergence to match the vertical and horizontal acceptances of the storage ring.

The last element must be a pulsed deflecting electrode that

TABLE IV: Injection matching fields

| | Sector 1 | Sector 2 |
|---|---|---|
| Electric field (MV/m) | 3.37 | 4.0 |
| Dipole coefficient ($m^{-1}$) | 158.5 | 38.2 |
| Radius (m) | -0.20 | 0.69 |
| Arc length (rad) | 0.397 | 0.426 |
| Phase advance (rad) | 1.57 | 1.55 |
| Focus parameter, $\beta$ (m) | 0.05 | 0.19 |

turns off after the bunch or bunches have entered. Several different injection protocols are available: a string of 158 $\mu$s pulses can be injected into the ring in less than the circulation period of 38 ms, or single bunches may be filled at any time by switching the pulsed deflecting electrode during the interval between bunches.

The injector guide field consists of two bending sectors, each an arc of about $\pi/8$ rad, arranged as shown in Fig.1. In each bending sector the field is configured to provide equal horizontal and vertical focusing. The phase advance of transverse motion is near $\pi/2$ in a sector; thus, it exchanges angle for displacement and changes the ratio of angle to displacement. Focusing strengths are adjusted to provide the required match between injecting beam and ring acceptance. The boundaries of the beam phase space are shown in Fig.13.

It was possible to choose the first sector to have radius and strength equal to that of the bend in the storage ring. The second sector must have larger aperture and radius and it must be pulsed to zero at the end of injection. Parameters of the injector guide field are shown in Table IV. The sum of the two inverse curves was made near zero so that the line of the decelerator is about parallel to the straight section of the synchrotron storage ring.

### C. Source and intensity

To estimate the number of molecules that can be decelerated, injected, and stored, we assume $^{14}N^2H_3$ source conditions similar to those reported by Crompvoets et al.[10] and by Bethlem et al.[24]: a pulsed jet source of 0.8% $^{14}N^2H_3$ seeded in 152 kPa (1140 Torr) of xenon (reservoir temperature 300 K) exiting through a circular 0.80 mm dia. orifice into vacuum. Following Crompvoets et al. [10], we assume that 15% of the molecules entering the decelerator are in the desired state. From the formulas in Miller[25], we find a flux of $4.4 \times 10^{18}$ $^{14}N^2H_3$ molecules $sr^{-1}s^{-1}$ in the desired $M$ state.

The decelerator's transverse emittance of $\pm 30$ mm-mr and momentum spread of $\pm 1\%$ at 90 m/s set a transverse acceptance from the 310 m/s jet source beam of $\pm 9$ mm-mr and momentum spread of $\pm 0.29\%$. If we assume an initial Gaussian velocity distribution with a mean of 310 m/s and a standard deviation of $\pm 20\%$, approximately 1.1 % of the molecules from the jet source fall within our decelerator momentum acceptance. With a pulse length of 158 $\mu$s, the intensity of the decelerated beam is roughly $6 \times 10^8$ molecules/pulse.

The horizontal acceptance of the storage ring matches the emittance of the decelerator and the vertical acceptance and momentum acceptance of the storage ring is about twice the emittance of the injected beam, so all $6 \times 10^8$ molecules/pulse should be captured and stored in a single bunch. If all sixty bunches are filled (over multiple turns) the total stored beam is $3.6 \times 10^{10}$ molecules and the circulating flux is $9.5 \times 10^{11}$ molecules/s.

### Acknowledgments

We thank Swapan Chattopadhyay and Ying Wu for early assistance with this work. Work on the synchrotron storage ring is supported by the Director, Office of Science, of the U.S. Department of Energy, and work on the linear decelerator is supported by the Director, Office of Science, Office of Basic Energy Sciences, of the U.S. Department of Energy; both under Contract No. DE-AC03-76SF00098.

[1] J. Doyle, B. Friedrich, J. Kim, and D. Patterson, Phys. Rev. A **52**, R2515 (1995).
[2] H. Bethlem, G. Berden, and G. Meijer, Phys. Rev. Lett. **83**, 1558 (1999).
[3] M. Gupta and D. Herschbach, J. Phys. Chem. A **103**, 10670 (1999).
[4] See, for example, J. T. Bahns, P. L. Gould, and W. C. Stwalley, in *Advances in Atomic Molecular and Optical Physics*, edited by B. Bederson and H.Walther (Academic, Orlando, 2000), vol. 42, p. 171.
[5] J. A. Maddi, T. Dinneen, and H. Gould, Phys. Rev. A **60**, 3882 (1999).
[6] J. Doyle and B. Friedrich, Nature **401**, 749 (1999).
[7] D. Auerbach, E. Bromberg, and L. Wharton, J. Chem. Phys. **45**, 2160 (1966).
[8] D. P. Katz, J. Chem. Phys. **107**, 8491 (1997).
[9] H. Loesch and B. Scheel, Phys. Rev. Lett. **85**, 2709 (2000).
[10] F. Crompvoets, H. Bethlem, R. Jongma, and G. Meijer, Nature **411**, 174 (2001).
[11] See, for example, H.F. Hess, Phys. Rev. B **34**, 3476 (1986).
[12] See, for example, W. Ketterle and N. J. V. Druten, in *Advances in Atomic, Molecular, and Optical Physics*, edited by B. Bederson and H.Walther (Academic, Orlando, 1996), vol. 37, p. 181.
[13] C.H.Townes and A. Schawlow, *Microwave Spectroscopy* (McGraw-Hill, New York, 1955).
[14] See, for example, J. Reuss, in *Atomic and Molecular Beam Methods*, edited by G. Scoles (Oxford, N.Y., 1988), p. 276.
[15] See, for example, P. W. Harland, W.-P. Hu, C. Vallance, and P. R. Brooks, Phys. Rev. A **60**, 3138 (1999).
[16] M. Kajita, T. Suzuki, H. Odashima, Y. Moriwaki, and

M. Tachikawa, Jpn. J. Appl. Phys. **40**, L1260 (2001).
[17] J. Kalnins, G. Lambertson, and H. Gould, Rev. Sci. Instr. **73**, 2557 (2002).
[18] H. Nishimura, in *Proc. Particle Accelerator Conf.* (IEEE, 2001), p. 3066.
[19] J. Amini (2001), private communication.
[20] D. Lide, ed., *Mean Free Path and Related Properties of Gases* (CRC Press, Boca Raton, 2002), chap. 6, p. 47, 83rd ed.
[21] J. L. Bohn, Phys. Rev. A **63**, 052714 (2001).
[22] M. Kajita, Eur. Phys. J. **D20**, 55 (2002).
[23] H. Bethlem, G. Berden, F. Crompvoerts, R. Jongma, A. van Roij, and G. Meijer, Nature **406**, 491 (2000).
[24] H. Bethlem, F. Crompvoerts, R. Jongma, S. Y. van de Meerakker, and G. Meijer, Phys. Rev. A **65**, 053416 (2002).
[25] D. Miller, in *Atomic and Molecular Beam Methods*, edited by G. Scoles (Oxford, N.Y., 1988), p. 14.